R & M No.3829

R & M No.3829

PROCUREMENT EXECUTIVE, MINISTRY OF DEFENCE

Aeronautical Research Council
Reports and Memoranda

VORTEX SHEDDING MECHANISMS IN RELATION TO TIP CLEARANCE FLOWS AND LOSSES IN AXIAL FANS

by

R.I. Lewis and E.H.C. Yeung

Newcastle University

London: Her Majesty's Stationery Office
£4 NET

VORTEX SHEDDING MECHANISMS IN RELATION TO TIP CLEARANCE FLOWS AND LOSSES IN AXIAL FANS

by

R. I. Lewis and E. H. C. Yeung

Newcastle University

REPORTS AND MEMORANDA No.3829*

May 1977

SUMMARY

This paper outlines the importance of tip leakage flows in axial fans as a source of loss and relates the dimensionless loss analytically to a range of dimensionless parameters by application of a jet loss theory due to Rains. Improved vortex shedding models are also presented. From these models theoretical predictions of lift coefficient reduction are compared with published experimental data for isolated rectangular plates, with experimental tests for a single aerofoil adjacent to a wall with an on-coming boundary layer and correlations due to Lakshminarayana.

---

* Replaces ARC 37359

LIST OF CONTENTS

		Page No.
1.0	INTRODUCTION	3
2.0	TIP LEAKAGE LOSSES IN AXIAL FANS	3
3.0	INFLUENCE OF TIP LEAKAGE LOSS UPON THE ANNULUS BOUNDARY LAYER	6
4.0	DISCRETIZATION METHOD FOR AEROFOILS WITH TIP VORTEX SHEDDING	7
	4.1 Vortex Lattice Method (VLM)	8
	4.2 Tip Vortex Method (TVM)	9
	4.3 Concentrated Tip Vortex Method (CTVM)	9
	4.4 Comparison between Theories (VLM) (TVM) and Experiment for Aerofoils	9
5.0	RECTANGULAR AEROFOIL IN WIND TUNNEL WITH FINITE TIP CLEARANCE	10
Conclusions		13
Notation		14
References		16
Illustrations		Figures 1-20
Detachable Abstract Cards		-

1.0 Introduction

In Section 2.0 relationships for tip leakage loss by the method of Rains[1], Vavra[2] and Hesselgreaves[3], are developed in a form which relates the losses to tip section duty coefficients ϕ,ψ and other important leading variables. Calculations for a typical engine cooling fan are then presented, revealing the dominating effect of tip leakage losses. Equations to calculate the increase of energy and displacement thickness due to tip clearance, by assuming that all the dissipative energy in the leakage jet is absorbed into the annulus boundary layer, are derived in Section 3.0.

Vortex shedding models are presented in Section 4.0, with minimal reference to the underlying mathematics, based upon (a) conventional lifting surface theory and (b) an improved model for the tip vortex representation. Computed results are compared with published experimental data for rectangular aerofoils of various aspect ratios.

Section 5.0 deals with the case of a single aerofoil located normal to a plane wall with on-coming boundary layers of two types and with tip clearances of varying magnitudes. The C_L distribution along the aerofoil and towards its tip is of main significance and also the influence of the tip vortex upon blade surface pressure distributions near to the blade end.

2.0 Tip Leakage Losses in Axial Fans

Following the method of Rains[1] and Vavra[2], Hesselgreaves[3] has derived the following expression for tip leakage energy loss in an axial fan with Z blades

$$\Delta E = \frac{2\sqrt{2}}{5} \tau \ell Z \rho W_\infty^3 C_{L\infty}^{3/2} \tag{1}$$

The underlying assumptions are

(a) a linear pressure distribution loading at the blade tip, Fig.(1)a, which results in a tip lift coefficient $C_{L\infty}$ defined

$$C_{L\infty} = \frac{L}{\frac{1}{2}\rho W_\infty^2 \ell} \tag{2}$$

(b) generation of tip leakage "jet" velocity v_t normal to the chord, Fig.(1)b , and given by

$$v_t = \sqrt{\frac{2}{\rho}(P_u - P_\ell)} \tag{2}$$

(c) tip leakage loss equal to the integrated "jet" kinetic energy $\frac{1}{2}\rho v_t^2$ over the whole blade chord.

Alternatively, pitch/chord ratio may be introduced, since

$$t = \frac{\pi D}{Z} \tag{3}$$

Hence

$$\Delta E = \frac{2\sqrt{2}}{5} \pi \rho \left(\frac{\tau}{D}\right)\left(\frac{\ell}{t}\right) D^2 W_\infty^3 C_{L\infty}^{3/2} \tag{4}$$

A convenient dimensionless tip leakage loss coefficient then follows:-

$$\Delta\bar{E} = \frac{\Delta E}{\frac{1}{2}\rho C_x^3 D^2} = \frac{4\sqrt{2}}{5} \pi \left(\frac{\tau}{D}\right)\left(\frac{\ell}{t}\right)\left(\frac{W_\infty}{C_x}\right)^3 C_{L\infty}^{3/2} \tag{5}$$

Dimensionless loss according to this simple theory is thus seen to depend, as one would expect, upon

$\frac{\tau}{D}$ - Dimensionless tip clearance

$\frac{t}{\ell}$ - Pitch chord ratio at the tip

$C_{L\infty}$ - Lift coefficient at the tip

$\left(\frac{W_\infty}{C_x}\right)$ - Velocity triangles at the tip

Now the actual and normalised velocity triangles for a fan rotor tip section are shown in Fig.(2), from which,

$$C_{L\infty} = 2\left(\frac{t}{\ell}\right)(\tan\beta_1 - \tan\beta_2)\cos\beta_\infty - C_D\tan\beta_\infty$$

$$\approx 2\left(\frac{t}{\ell}\right)\psi\{\phi^2+(1-\tfrac{\psi}{2})^2\}^{-\frac{1}{2}}$$

where, in the second form, the C_D term has been neglected.

Also from Fig.(2) we can show that

$$\frac{W_\infty}{C_x} = \frac{1}{\phi}\{\phi^2 + (1-\tfrac{\psi}{2})^2\}^{\frac{1}{2}}$$

so that finally

$$\Delta\bar{E} = \frac{16}{5}\pi\left(\frac{\tau}{D}\right)\left(\frac{t}{\ell}\right)^{\frac{1}{2}}\frac{\psi^{3/2}}{\phi^3}\{\phi^2 + (1-\tfrac{\psi}{2})^2\}^{3/4} \qquad (6)a$$

$$= f\left(\frac{\tau}{D}, \frac{t}{\ell}, \phi, \psi\right) \qquad (6)b$$

In this form we see the normalised tip leakage losses depend upon two obviously important geometrical parameters, gap ratio and pitch/chord ratio but also upon the duty coefficients to which the blade tip aerofoils are subjected

$$\phi = \frac{C_x}{U_t}, \qquad \psi = \frac{1}{\rho}\frac{\Delta p_o}{U_t^2}$$

Whatever credibility is assigned to this theoretical model, which does seem to yield reasonable results[3] in comparison with experiments, this simple analysis demonstrates that duty at the tip is of equal significance to other geometrical or aerodynamic considerations. Thus choice of (ϕ,ψ) at the tip can have considerable influence upon $\Delta\bar{E}$.

However, one practical expectation is that the design $C_{L\infty}$ at the tip may not be achieved due to tip unloading, in which case equation (5) would over estimate $\Delta\bar{E}$. One important aspect of this research is to establish the magnitude of this effect in relation to assumptions (a) to (c) above.

A second point to raise is that $\Delta\bar{E}$ as defined does not relate the tip leakage loss to the total flow power input. It is therefore slightly more convenient to define an alternative normalised loss as follows,

$$TL = \frac{\Delta E}{\text{Flow power input}}$$

$$= \frac{\Delta E}{\rho C_x \pi (r_t^2 - r_h^2)\Delta p_o}$$

assuming constant input head Δp_o for all radii. After manipulation

$$TL = \frac{32}{5(1-h^2)}\left(\frac{\tau}{D}\right)\left(\frac{t}{\ell}\right)^{\frac{1}{2}} \frac{\psi^{\frac{1}{2}}}{\phi}\left\{\phi^2+\left(1-\frac{\psi}{2}\right)^2\right\}^{3/4} \quad (7)a$$

$$= f\left(\frac{\tau}{D}, \frac{t}{\ell}, h, \phi, \psi\right) \quad (7)b$$

Thus the additional geometrical variable, hub/tip ratio h is introduced. It should be noted that this also implies the importance of blade aspect ratio defined

$$\frac{H}{\ell} = \frac{D}{2}\,\frac{(1-h)}{\ell} \quad (8)$$

which is a more significant parameter when seeking to investigate tip leakage losses by cascade tests. τ/ℓ is also then a more appropriate gap ratio parameter. Equation (7) then transforms to

$$TL = \frac{16}{5}\left(\frac{1}{1+h}\right)\left(\frac{\tau}{\ell}\right)\left(\frac{\ell}{H}\right)\left(\frac{t}{\ell}\right)^{\frac{1}{2}} \frac{\psi^{\frac{1}{2}}}{\phi}\left\{\phi^2+\left(1-\frac{\psi}{2}\right)^2\right\}^{3/4} \quad (9)$$

For the machine the dimensionless loss, equation (5), transforms to

$$\Delta\bar{E}_F = \Delta E/\tfrac{1}{2}\rho C_x^3 D^2$$

$$= \frac{8}{5}\pi(1-h)\left(\frac{\tau}{\ell}\right)\left(\frac{\ell}{t}\right)\left(\frac{\ell}{H}\right)\frac{\psi^{3/2}}{\phi^3}\left\{\phi^2+\left(1-\frac{\psi}{2}\right)^2\right\}^{3/4} \quad (10)$$

and for a cascade equation (1) transforms to a dimensionless loss for each blade of the cascade given by

$$\Delta\bar{E}_{C_1} = \Delta E/\tfrac{1}{2}\rho C_x^3 H^2 \quad (11)a$$

$$= \frac{4\sqrt{2}}{5}\left(\frac{\tau}{\ell}\right)\left(\frac{\ell}{H}\right)^2\left(\frac{W_\infty}{C_x}\right)^3 C_{L\infty}^{3/2} \quad (11)b$$

If we apply this cascade loss to a fan with blades of height H and with tip duty (ϕ,ψ), then the final form of loss coefficient per blade becomes

$$\Delta\bar{E}_{C_1} = \frac{16}{5}\left(\frac{\tau}{\ell}\right)\left(\frac{\ell}{H}\right)^2\left(\frac{t}{\ell}\right)^{3/2}\frac{\psi^{3/2}}{\phi^3}\left\{\phi^2+\left(1-\frac{\psi}{2}\right)^2\right\}^{3/4} \quad (12)$$

This form of a dimensionless loss coefficient for a single blade based upon a common definition, equation (11)a, thus suits both fan and cascade equivalent.

To achieve this common definition, however, it becomes clear that in addition to the obvious relevant cascade parameters τ/ℓ, H/ℓ, and t/ℓ, the duty coefficients (ϕ,ψ) of the fan, for which the cascade test is to be performed are equally relevant.

Equations (11)b and (12) are however directly equivalent and (11)b is more useful for extracting results from cascade considerations alone. Equation (12) simply reinforces the important point that duty selection (ϕ,ψ) at the blade tip plays a vital role in determining the value of tip leakage losses.

Although the theory chosen may be open to criticism, these particular fundamental points remain basic and worthy of special note.

Based upon this formulation and a computer aided design method developed in Ref.4, Fig.(3) illustrates the catastrophic effect of tip leakage loss upon the performance of a typical engine cooling fan.

3.0 Influence of Tip Leakage Loss upon the Annulus Boundary Layer

Tip leakage losses result not only in reduced efficiency but also in complex annulus boundary layer flows. The energy decrement caused by the tip leakage loss can lead to rapid growth of the casing annulus boundary layer, well in excess of that due to wall frictional effects, and to large local disturbances at the blade tips which move circumferentially with the rotor. The models outlined in the remaining sections were developed to handle this type of flow regime with increasing accuracy. In the present section a simple approach is adopted, based upon power law profiles, to provide a structure for handling the design and performance analysis considerations in a practicable way. At best, the following analysis is an expedient resulting in simplicity, but with scope for more advanced analysis as the loss mechanism becomes more fully understood.

For a 1/7th power law profile, all other boundary layer parameters may be related to the thickness δ directly through

$$\left.\begin{aligned} \delta^* &= \int_0^\delta \left(1 - \frac{c_x}{C_x}\right) dy = \frac{1}{8}\delta \\ \theta &= \int_0^\delta \frac{c_x}{C_x}\left(1 - \frac{c_x}{C_x}\right) dy = \frac{7}{72}\delta \\ \delta^{**} &= \int_0^\delta \frac{c_x}{C_x}\left\{1 - \left(\frac{c_x}{C_x}\right)^2\right\} dy = \frac{7}{40}\delta \end{aligned}\right\} \qquad (13)$$

where

$$\frac{c_x}{C_x} = \left(\frac{y}{\delta}\right)^{1/7} \qquad (14)$$

Thus the change in displacement thickness between inlet and outlet at the fan tip can be expressed

$$\delta_2^* = \delta_1^* + \frac{5}{7}(\delta_2^{**} - \delta_1^{**}) \qquad (15)$$

where $(\delta_2^{**} - \delta_1^{**})$ is the change in energy thickness, which we will assume is entirely due to tip leakage energy loss in this instance.

Thus the change in the energy decrement of the boundary layer can be related directly to the tip leakage loss ΔE as follows

$$\Delta E = \tfrac{1}{2}\rho\pi D\left[\int_0^{\delta_2} c_{x_2}\left\{\frac{C_{x_2}^2 - c_{x_2}^2}{\cos^2\beta_\infty}\right\} dy - \int_0^{\delta_1} c_{x_1}\left\{\frac{C_{x_1}^2 - c_{x_1}^2}{\cos^2\beta_\infty}\right\} dy\right] \qquad (16)$$

$$= \tfrac{1}{2}\rho C_x{}^3 \pi D(\delta_2^{**} - \delta_1^{**})\sec^2\beta_\infty$$

A conceptual problem arises here since the tip leakage loss ΔE is not simply absorbed into the energy decrement of the axial velocity component of the annulus boundary layer, but into the relative boundary layer as seen by the blade tips. The assumption implicit in equation (16) is that ΔE is deposited as a decrement to the relative vector mean velocity W_∞ at the blade tip, which results in the appearance of $\sec\beta_\infty$ as an approximation towards this hypothesis.

The introduction of equations (6)a and (13) then results finally in

$$\frac{\delta_2^* - \delta_1^*}{D} = \left(\frac{\tau}{D}\right)\left(\frac{t}{\ell}\right)^{\frac{1}{2}} \frac{16}{7}\frac{\Psi^{3/2}}{\phi}\left\{\phi^2 + \left(1 - \frac{\Psi}{2}\right)^2\right\}^{-1/4} \qquad (17)$$

For the convenience of manual calculations the following universal functions have been plotted in Figs. (4) and (5).

$$\left.\begin{aligned} TL\left\{\frac{1-h^2}{\left(\frac{\tau}{D}\right)\left(\frac{t}{\ell}\right)^{\frac{1}{2}}}\right\} &= \frac{32}{5}\frac{\Psi^{\frac{1}{2}}}{\phi}\left\{\phi^2 + \left(1 - \frac{\Psi}{2}\right)^2\right\}^{3/4} \\ \left(\frac{\delta_2^* - \delta_1^*}{D}\right) \Big/ \left\{\left(\frac{\tau}{D}\right)\left(\frac{t}{\ell}\right)^{\frac{1}{2}}\right\} &= \frac{16}{7}\frac{\Psi^{3/2}}{\phi}\left\{\phi^2 + \left(1 - \frac{\Psi}{2}\right)^2\right\}^{-1/4} \end{aligned}\right\} \qquad (18)$$

Thus for any given tip duty (ϕ,Ψ) one can quickly estimate the tip leakage loss and consequent increase in energy or displacement thickness for particular gap ratios or pitch/chord ratios.

4.0 Discretization Method for Aerofoils with Tip Vortex Shedding

Most numerical methods for calculation of aerofoil loading are based on the well known fluid dynamic modelling techniques for incompressible fluids[5], whereby the aerofoil and its vortex wake are represented by vorticity distributions bound to the aerofoil or trailing downstream. For thin aerofoils the flow may be represented with good approximation by a bound vorticity sheet on the camber surface combined with a vortex wake shed partly at the aerofoil tip but also across the entire trailing edge, Fig.(6). The induced velocities normal to the camber surface due to the entire vorticity structure must be zero at all points, to satisfy the surface boundary condition of parallel flow. For thin aerofoils this condition may be expressed analytically as follows:-

$$\frac{w(x,y) + W}{u(x,y) + U} = \frac{d}{dx}(Z_s(x,y)) \tag{19}$$

where $u(x,y)$, $w(x,y)$ are vorticity induced velocities and U,W are main stream velocities, in the x and z direction. $Z_s(x,y)$ is the camber surface of the aerofoil.

The downwash at (x,y) due to the whole vortex system is then given by the integral equation

$$w(x,y) = \iint_s K\{(x,y), (x',y')\}\gamma(x'y')dx'dy' \tag{20}$$

where $\gamma(x',y')$ is the vorticity of an element at (x',y') and $K\{(x,y),(x',y')\}$ is the coupling coefficient connecting points (x,y) and (x',y').

Figure (6) illustrates three models of increasing complexity and accuracy, which were adopted for calculations presented in the following subsections. Yeung[5] has provided full analytical details of the appropriate forms of the governing equations (19) and (20), and selected final results only will be presented here. Figures (6)a, (6)b and (6)c represent the Vortex Lattice Method (VLM), the Tip Vortex Method (TVM) and the Concentrated Tip Vortex Method (CTVM). These are dealt with in Sections (4.1), (4.2) and (4.3) respectively.

4.1 Vortex Lattice Method (VLM)

This most common method of lifting surface analysis can be applied to thin aerofoils of small camber and twist. The projection of the aerofoil on the x-y plane is divided into small rectangular elements by grid lines parallel to span and chord, Fig.(7). A horseshoe vortex is placed on each element, comprising the bound vortex $\gamma_{ij}\Delta x_{ij}$ located at the 1/4 chord position of element (i,j) and two trailing vortices extending to infinity downstream. The boundary conditions of parallel flow is satisfied at each control point P_{ij}, located at the 3/4 chord line of each element. At these locations the downwash induced by the horseshoe vortex systems is given by

$$\begin{aligned} w_{ij} &= \sum_{n=1}^{N}\sum_{m=1}^{M} w_{ij,mn} \\ &= \sum_{n=1}^{N}\sum_{m=1}^{M} K_{ij,mn}\,\gamma_{mn} \end{aligned} \tag{21}$$

which is the numerical equivalent of equation (20). $w_{ij,mn}$ is the induced downwash at element (i,j) due to the horseshoe vortex element at (m,n) and $K_{ij,mn}$ is the coupling coefficient.

For this system, equation (19) reduces to

$$\sum_{n=1}^{N}\sum_{m=1}^{M} \gamma_{mn} K_{ij,mn} = \{\frac{d}{dx}(Z_{sij}) - \tan\alpha\}U \tag{22}$$

A set of linear equations can then be established which provide a solution for γ_{mn} and hence the full flow field.

With the (VLM), no special consideration is given to the tip vortex development. The tip horseshoe vortex provides for this process but with the constraint that the tip vortex is assumed to lie along the x axis, Fig.(7).

4.2 Tip Vortex Method (TVM)

As will be seen later in Section (5.0) the (VLM) fails to predict with sufficient accuracy the performance of low aspect ratio aerofoils. Errors are largely due to neglect of the presence of the cumulatively developed rolled up tip vortices[6].

To model the rolling up process would seem excessively complex involving the adoption of a time marching approach. An improved compromise model has therefore been adopted similar to (VLM) in all respects except for the treatment of the tip section. In addition to the trailing edge trailing vortex sheet, two vortex sheets are assumed to be shed from the tips of the aerofoil, Fig.(6)b, located in the (x,z) plane, and trailing downstream at an angle β_i with the x axis, Fig.(8). For all elements other than the tips, the bound and shed vortices are assumed to lie on the x-y plane.

$$\beta_i = \{\tan^{-1}\frac{d}{dx}(Z_{sij}) + \alpha\}/2 \text{ for } j = 1 \text{ or } N \qquad (23)$$

and each elementary vortex is assumed to flow to infinity without change of direction or strength. A governing equation of similar form to equation (21) is obtained with the addition of a special term to include the tip vortices.

4.3 Concentrated Tip Vortex Method (CTVM)

A further advance towards the true fluid mechanism is under investigation by the model illustrated in Fig.(6)c. The vortex sheet shed from the tip is assumed to roll up fairly rapidly into a concentrated tip vortex, whose strength develops cumulatively due to the feeding process. As before the feeding vortices leave the trailing edge with angle β_i in the (x,z) plane but it is now possible also to model the rolling up process by allowing the tip vortex to be inclined to the (x,z) plane by the angle ε as seen in plane view, Fig.(6)c. Experimental results indicate that such a model may be close to the truth for aerofoils or for fan cascades with fairly large clearances.

4.4 Comparison between Theories (VLM) (TVM) and Experiment for Aerofoils

Figures (9) and (10) show the calculated spanwise circulation distributions for flat plate aerofoils of rectangular plan form with an angle of attack of 4°. For computational speed, the grid was limited to six chordwise segments and fifteen spanwise segments with the plane of symmetry at mid-span. Estimated errors due to grid limitations are within 2%.

Computed results in Fig.(9) are normalised against the mid-span circulation which helps to bring out the effects of aspect ratio upon the spanwise distribution of loading. In both Figs. (9) and (10) half span results are plotted side by side for (VLM) and (TVM) for the purposes of comparison.

An aerofoil of infinite span will obviously have constant circulation equal to that of a two-dimensional aerofoil as indicated by the progressive trend of these curves for aspect ratios increasing through 2, 6 to 20. The two methods are in good agreement for these high aspect ratios.

At the other extreme of diminishing aspect ratios from 0.5, 0.25 to 0.06, however, the theories disagree. The simple (VLM) approaches a limiting form of elliptical loading. On the other hand the (TVM), which is more realistic to the true fluid flow situation, suggests that in the limit of infinitely small aspect ratio, the circulation would be constant across infinitesimal span.

Figure (10), in which the blade circulation is normalised against the two-dimensional circulation ($s/\ell = \infty$), further illustrates this point, but also reveals the lift reduction experienced at reducing values of aspect ratio.

Figure (11) reveals that the spanwise distribution of lift coefficient, normalised against the overall lift coefficient, is independent of angle of attack according to (VLM). The (TVM) theory however, predicts considerable variation in the normalised lift coefficient which is very similar in its trend to the experimental results published by Holme[7], Fig.(12). The main discrepancy between (TVM) and experiment here occurs in the region very close to the aerofoil tip, where strong suction peaks were observed experimentally. These are believed to be due to the growth of the concentrated rolled up tip vortex adjacent to the suction surface of the aerofoil tip, giving rise to a local reduction in static pressure. It was on the evidence of these observations that the more advanced (CTVM) fluid dynamic model was subsequently developed by the present authors. It is of interest to observe that these disturbances are largely absent for small angles of attack since, as one might expect, the mainstream convection velocities predominate in comparison with vortex induced velocities. In these circumstances rolling up of the vortex sheets would take place more slowly further downstream of the aerofoil.

Actual lift coefficients versus angle of attack, predicted by (VLM) and (TVM), are compared in Fig.(13) with experimental results reported by Küchemann[8]. For aerofoils with large aspect ratios, the two methods give nearly identical predictions and agree fairly well with the experimental tests for angles below stall. However, deviation between the two theories worsens as the aspect ratio is reduced. For small aspect ratios (TVM) invariably gives a much better prediction than (VLM) and is in good accord with experiment even for an aspect ratio $s/\ell = 0.5$.

Thus these calculations establish the Tip Vortex Method (TVM) as undoubtedly the superior model for aerofoils of widely varying aspect ratio and as an accurate prediction method for overall lift coefficient, with good promise for prediction of spanwise variations. The test to which the method has been subjected would seem to the authors excessively more rigorous than that called for when dealing with tip leakage problems and offers considerable encouragement for further progress in this field.

Since the preceding research was confined to flat plate aerofoils, a further computation was completed for Clark Y aerofoils at various angles of attack and for a range of aspect of ratios, Fig.(14). The (TVM) theory gives extremely good agreement with published experiments in all cases for unstalled flow. It is of interest to observe the inhibition of stall at low aspect ratios, e.g. $s/\ell = 0.5$, for incidence angles as high as 25° due to the reduction in C_L and the influence of tip vortex induced velocities.

5.0 Rectangular Aerofoil in Wind Tunnel with Finite Tip Clearance

The aerodynamics of tip clearanceflows have already received much attention by early research workers such as Grammel[10], Prandtl and Betz[11]. More recently Lakshminarayana and Horlock[12] have attempted a lifting line approach which assumes constant spanwise circulation, with a fraction only of the bound circulation shed from the blade tip. For small gaps the assumption is then made that the highly viscous processes in the tip region result in complex vorticity generation mechanisms which mask the inviscid mechanisms assumed by the present authors. For extremely small tip clearances the assumption of constant circulation may prove valid but the evidence of the preceding sections indicates otherwise for blade rows with large tip clearances.

Sugiyama[13] has adopted a more advanced lifting surface analysis in which a chordwise vorticity distribution was prescribed but with constant strength in the spanwise direction. Downwash boundary conditions were satisfied at the mid-span position only, however, in his analysis.

Experiments were performed[5] using two different wall boundary layers in the approach flows, Fig.(15), both approaching the 1/7th power law. The wind tunnel natural boundary layer was left unchanged in experiment A but a very much thicker boundary layer was generated by means of an upstream graded grid to perform experiment B.

Figure (16) summarises all the available experimental data including the "K" values, retained lift at the tip, published by Lakshminarayana and Horlock[12], concerning the dependency of (endwall lift/tip section lift) upon the gap ratio τ/ℓ. The endwall lift is that which is assumed to be retained by the fluid adjacent to the endwall surface as a result of the highly viscous flows in the gap, to which reference was made earlier. In the present work, static pressure tappings were located on the end wall around the contour which would be marked out by the blade surface for the case of zero tip clearance. From endwall pressure plots it was thus possible to calculate the lift coefficient upon the sheet of fluid adjacent to the end wall and occupying the space of the aerofoil contour. This work was undertaken originally in order to attempt to improve upon Rain's theory[1] discussed in Section 2.0. However, it has subsequently proved useful as a means for correlating the present work with that of Lakshminarayana and Horlock[12].

Figure (16) reveals fair correlation over a wide range of gap ratios, with maximum scatter occurring for values of τ/ℓ less than 0.05. At these very low tip clearances there is evidently a predominating viscous influence. The ratio, which represents, in effect, the fraction of blade tip lift retained by the viscous fluid in the gap, can be expressed empirically by

$$K = e^{-14\,\tau/\ell} \qquad (24)$$

Boundary layer thickness appears to have had minimal effect upon this correlation.

This curve agrees especially well at low and high values of gap ratio and could form a useful technique for improving upon the Rain's jet kinetic energy analysis.

The discretization method described in Section (4.0) has been extended by the present authors[5] to tip clearance analysis. As illustrated by Fig.(17), mirror image method was used to model end wall interference effects. For reduction of computing time, however, single reflections of the half span only were included since the predominating influence is in fact the vortex flow local to the wall. This seems to be a reasonable simplification.

The present model is in fact a modified TVM. The only differences between the two are the strength of the tip vortices and their direction. From equation (24) the shed tip vorticity is:

$$(\gamma_{tip})_i = (1-K)\,\gamma_{ij} \qquad j = 1 \text{ or } N \qquad (25)$$

The jet velocity, v_t, averaged across the gap is approximately equal to

$$(v_t)_i = \frac{W - c_{fi}\frac{2\tau}{\delta_{ti}}\left(U - \frac{Ky_{ij}}{2}\right)^2 + 2UKy_{ij}}{1 + c_f\frac{2\tau}{\delta_{ti}}} \qquad (26)$$

where

c_f is friction factor

W, U are stream velocity components in z and x directions

τ is gap height

and δ_t is thickness of the aerofoil

The direction of the tip vortex is approximated to

$$\beta_i = \left(\tan^{-1}\frac{d}{dx}(Z_{sij}) + \frac{(Ut)_i}{U - \frac{Ky_{ij}}{2}}\right)\Big/2 \qquad (27)$$

Figure (18) shows a comparison of the percentage reduction in total lift versus gap chord ratio derived experimentally by Lakshminarayana and Horlock[12] with three theories. (VLM) and (TVM) agree adequately for large gap ratios of 0.2 as one might expect but show complete inadequacy to deal with smaller gap chord ratios even in the modest range 0.05 to 0.15. The modified TVM outlined above, however, reveals close agreement over the whole range of gap ratios.

Experiments performed by Yeung[5] with a 29° circular camber aerofoil, NACA 65-008 base profile, at 14.6° angle of attack showed fairly similar characteristics, Figs. (19) and (20), the main differences occurring at low gap ratios. In these experiments an optimum gap ratio was found in the region of 0.03. For $\tau/\ell < 0.06$ a slight increase of total lift coefficient occurred compared with the value for zero clearance. The influence of the thicker boundary layer, Case B, was found to be marginally worse at high gap/chord ratios in relation to the percentage reduction in lift coefficient compared with the zero gap case.

Since the aerofoil was at fairly high angle of attack and believed to be separating even with zero clearance, no comparison is being made between the theory and the experiment. The discretization technique is an inviscid analysis and cannot predict the performance accurately when the aerofoil separates.

Further experimental work in this area needs to be undertaken to determine the strength and location of the tip vortex and the nature of the roll up process. A more appropriate model similar to (CTVM), Fig.(6)c, is required to cope with the presence of the vortex core located adjacent to the suction surface.

CONCLUSIONS

A simple equation to determine the tip leakage loss in terms of duty coefficient and geometrical parameters at the tip has been derived based on the jet theory. By assuming that all the energy in the tip leakage jet is absorbed into the annular wall boundary layer, equations for calculating the energy and displacement thickness growth were also derived. Calculations for a typical fan reveal the dominating effect of tip leakage.

A three-dimensional calculation method is developed which can be applied to a single aerofoil in a uniform free stream or in a wind tunnel with a clearance gap. The analysis for an aerofoil in a uniform free stream demonstrates the importance of the pair of tip vortices. Experimental evidence from tip clearance tests show that there is a variation of pressure across the gap and a reduction in lift coefficient at the tip, compared with the value of lift coefficient with no gap, depending on the aspect ratio and the size of the gap. The energy in the tip leakage jet is hence likely to be smaller than given by the jet theory. The indirect effect of tip clearance, the shedding of circulation along the blade span, contributes the other portion of the loss. At small gap, the total loss is likely to be approximately equal to that given by the jet theory. For large gaps one can no longer afford to ignore the complex effects of the vortex development and its associated induced velocities.

NOTATION

C_L	lift coefficient
C_D	drag coefficient
C_x	axial velocity in main stream
c_x	axial velocity
c_f	friction factor
D	diameter or drag
ΔE	tip leakage loss
h	hub tip ratio
H	blade height
K	coupling coefficient, or ratio of lift on end wall/ratio of lift on blade tip
ℓ	chord length
L	lifting force
TL	normalized tip leakage loss $\frac{\Delta E}{\text{Flow power input}}$
Q	velocity
U,V,W	velocity component in x,y,z directions
Z	no of blades
$Z_S(x,y)$	camber surface
p	static pressure
p_o	total pressure
Δp	static pressure change
Δp_o	total pressure change
r	radius
s	span
t	pitch
U	blade speed
u,v,w	induced velocity components in x,y,z directions
α,β,ε	flow angles
γ	stagger angle or vorticity

δ	boundary layer thickness
δ^*	displacement thickness
δ^{**}	K.E. thickness
δ_t	blade thickness
θ	momentum thickness
τ	tip clearance
ψ	head coefficient $\frac{\Delta p_o}{\rho U^2}$
ϕ	flow coefficient $\frac{C_x}{U}$

subscript

1,2	inlet, outlet
i,j,m,n	grid number in x,y direction
h	hub
t	tip
u	upper surface
ℓ	lower surface
∞	mean value

REFERENCES

1. Rains, D.A. — Tip clearance problems in axial compressors. A.E.C. R & D Report No. K-1682. Union Carbide Corporation, Nuclear Division, 1968.

2. Vavra, M.H. — Aero-thermodynamics and flow in turbomachines, p.381. New York, John Wiley & Sons, Inc., 1960.

3. Hesselgreaves, J.E. — A Correlation of tip-clearance/efficiency measurements on mixed-flow and axial-flow turbomachines. NEL Report No. 423, 1969.

4. Lewis, R.I. — A method for detailed performance prediction of rotor only axial fans with computer aid. Conference on Computer Aided Design of Pumps and Fans, I.Mech.E., Sept., 1973.

5. Yeung, H.C. — Ph.D. Thesis in preparation.

6. Fage, A. and Simmons, L.F.G. — An investigation of the air-flow pattern in the wake of an aerofoil of finite span. ARC R & M 951, 1925.

7. Holme, O.A.M. — Measurement of pressure distribution on rectangular wings of different aspect ratio. Flygtekniska Försöksanstalten FFA Meddelande NR 37 Stockholm 1950.

8. Küchemann, D. — A simple method for calculating the spanwise and chordwise loading on straight and swept wings of any given aspect ratio at subsonic speeds. ARC R & M 2935, 1952.

9. Zimmerman, C.H. — Characteristics of Clark Y aerofoils of small aspect ratio. NACA Report No. 431, 1932.

10. Grammel, R. — Die hydrodynamischen Grundlagen des Fluges p. 84 F. Vieweg. Braunschweig, 1917.

11. Prandtl, L. and Betz, A. — Vier Abhandlungen zur Hydrodynamik und Aerodynamik p.52. Selbstverlag der Kaiser Wilhelm-Instituts für Strömungforschung, Göttingen, 1927.

12. Lakshminarayana, B. and Horlock, J.H. — Tip clearance flow and losses for an isolated compressor blade. ARC R & M 3316, June 1962.

13. Sugiyama, Y. — A theory for rectangular wings with small tip clearance in a channel. Aero Quarterly Vol.24, pp.103-119, May 1973.

14. Hawthorne, W.R. — Rotational flow through cascade Pt. I. The component of vorticity. Quart. J. of Mech. & Applied Math., Vol.VIII, Pt.3, pp.266-279, 1955.

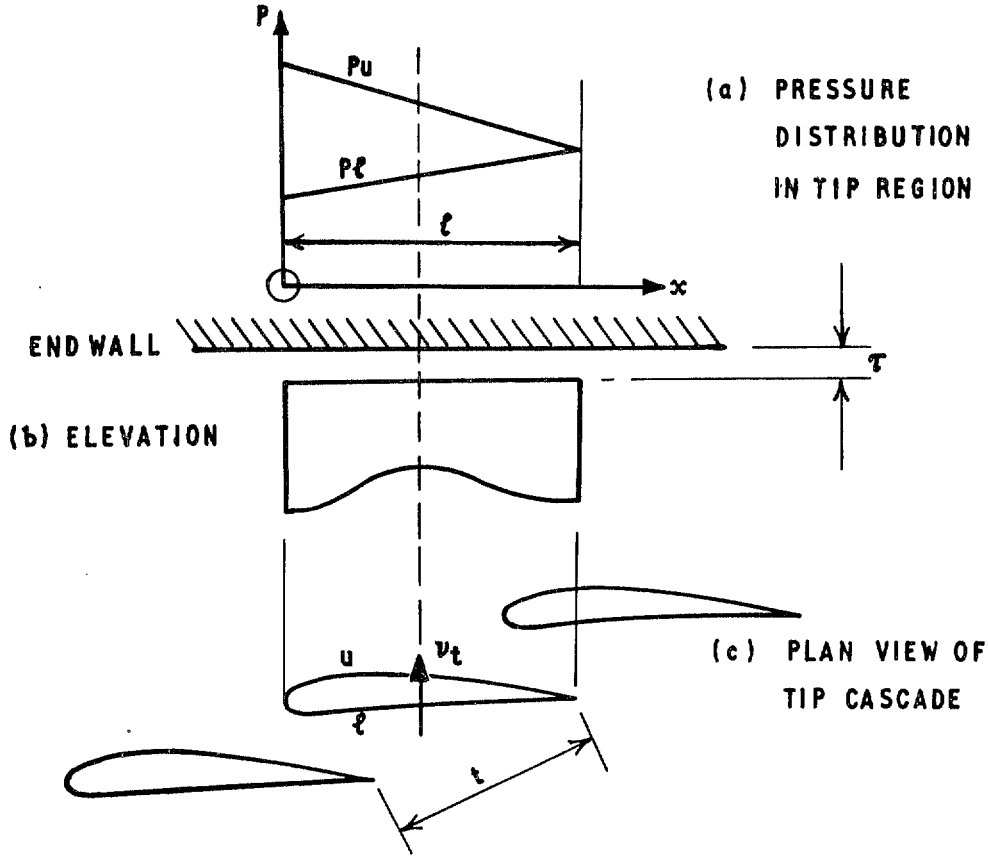

Fig 1a-c Tip clearance and blade geometry

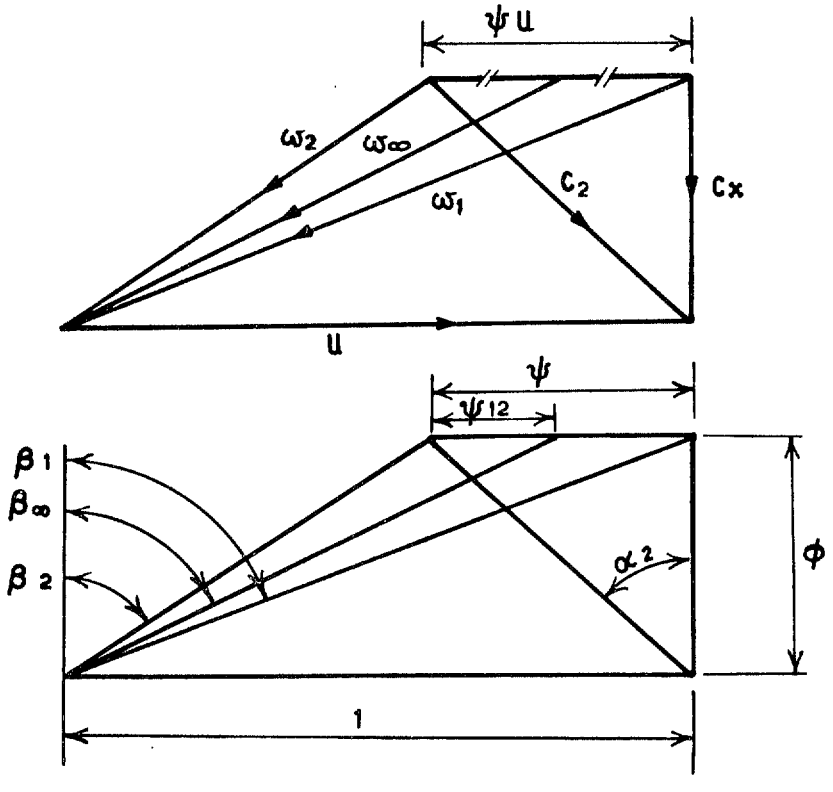

Fig 2

Fig 3

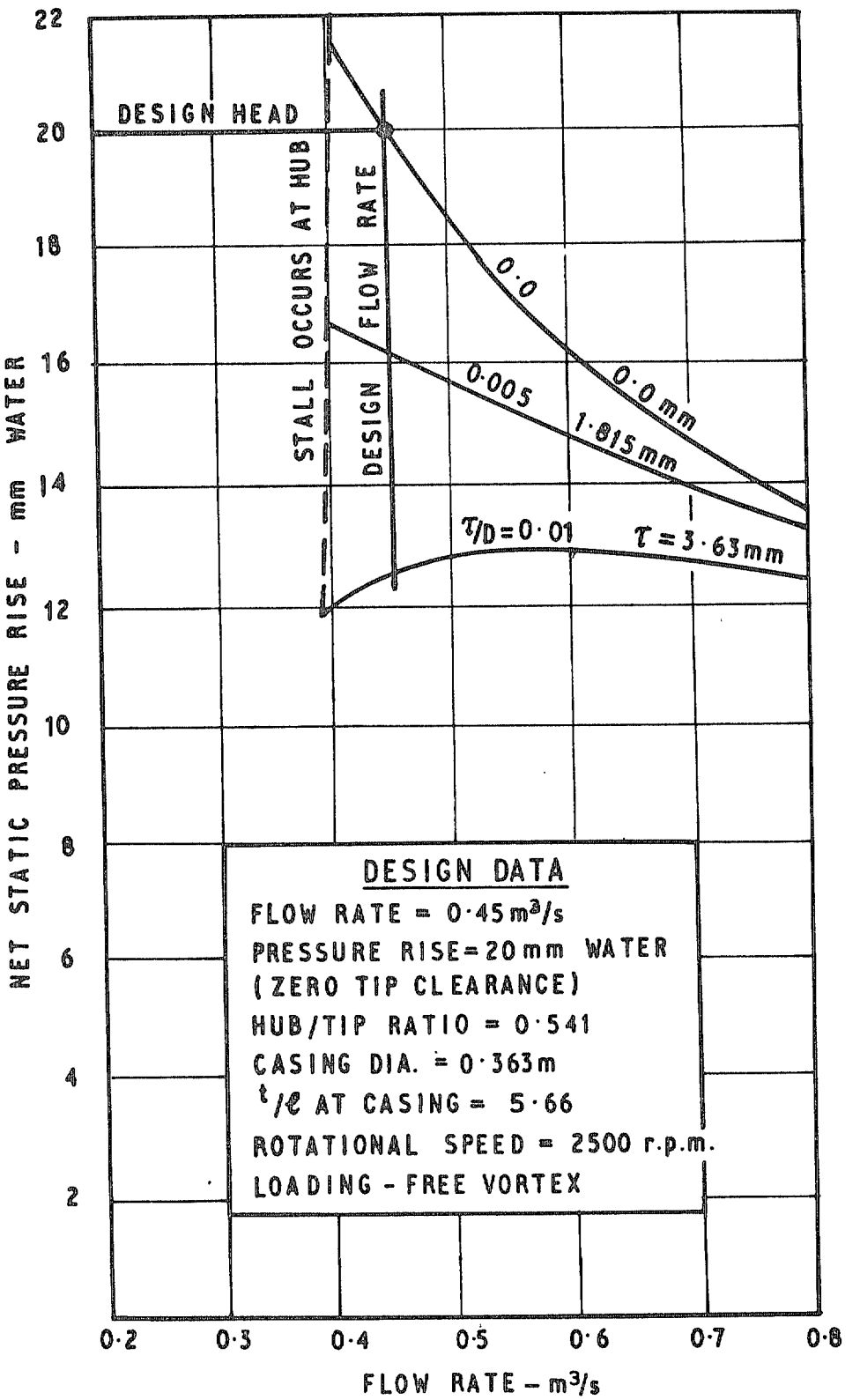

Fig 3 Effect of tip clearance upon typical free vortex axial fan characteristics

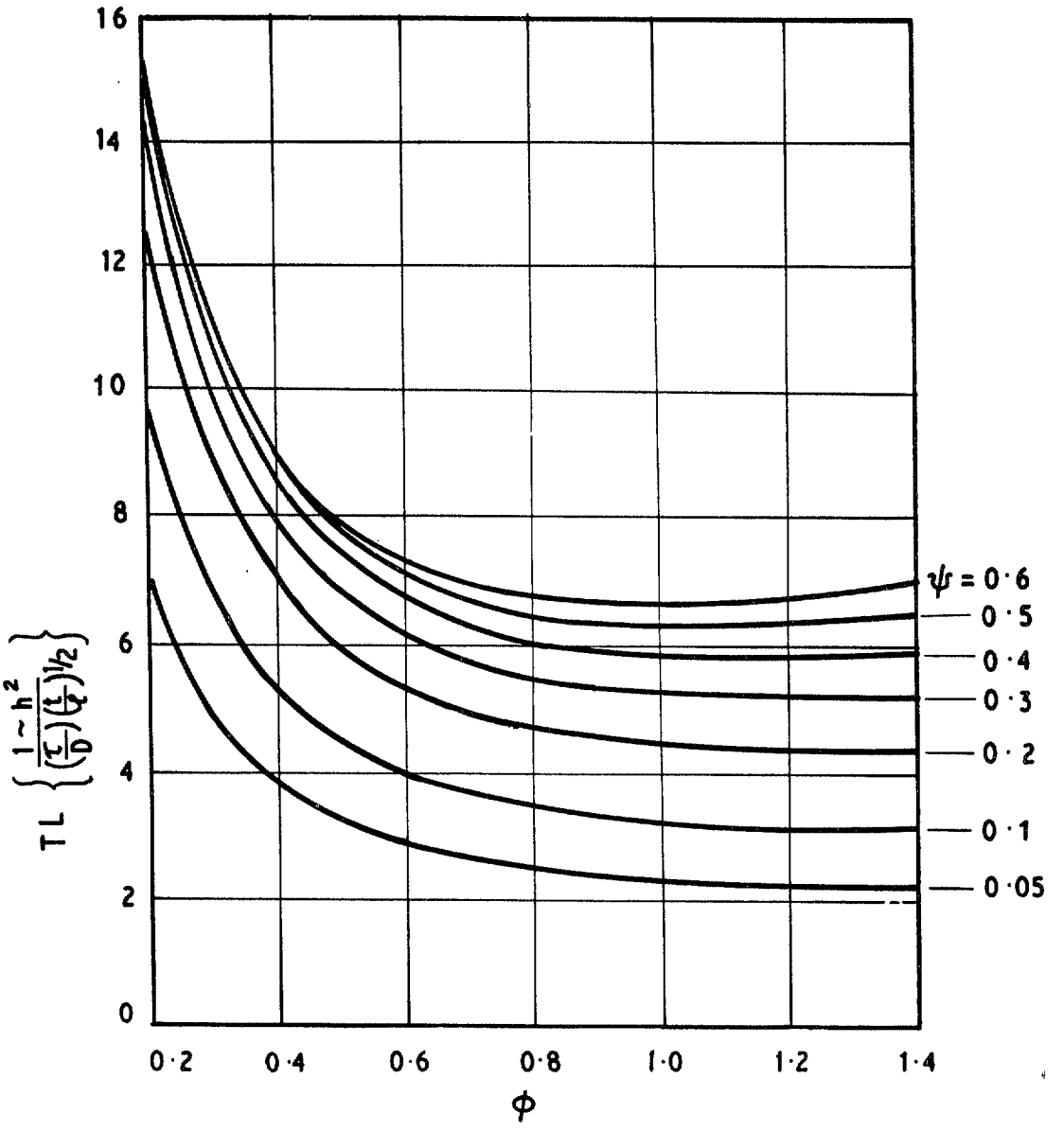

Fig 4 Tip leakage loss parameter for fans with given tip duty coefficients (ϕ, ψ)

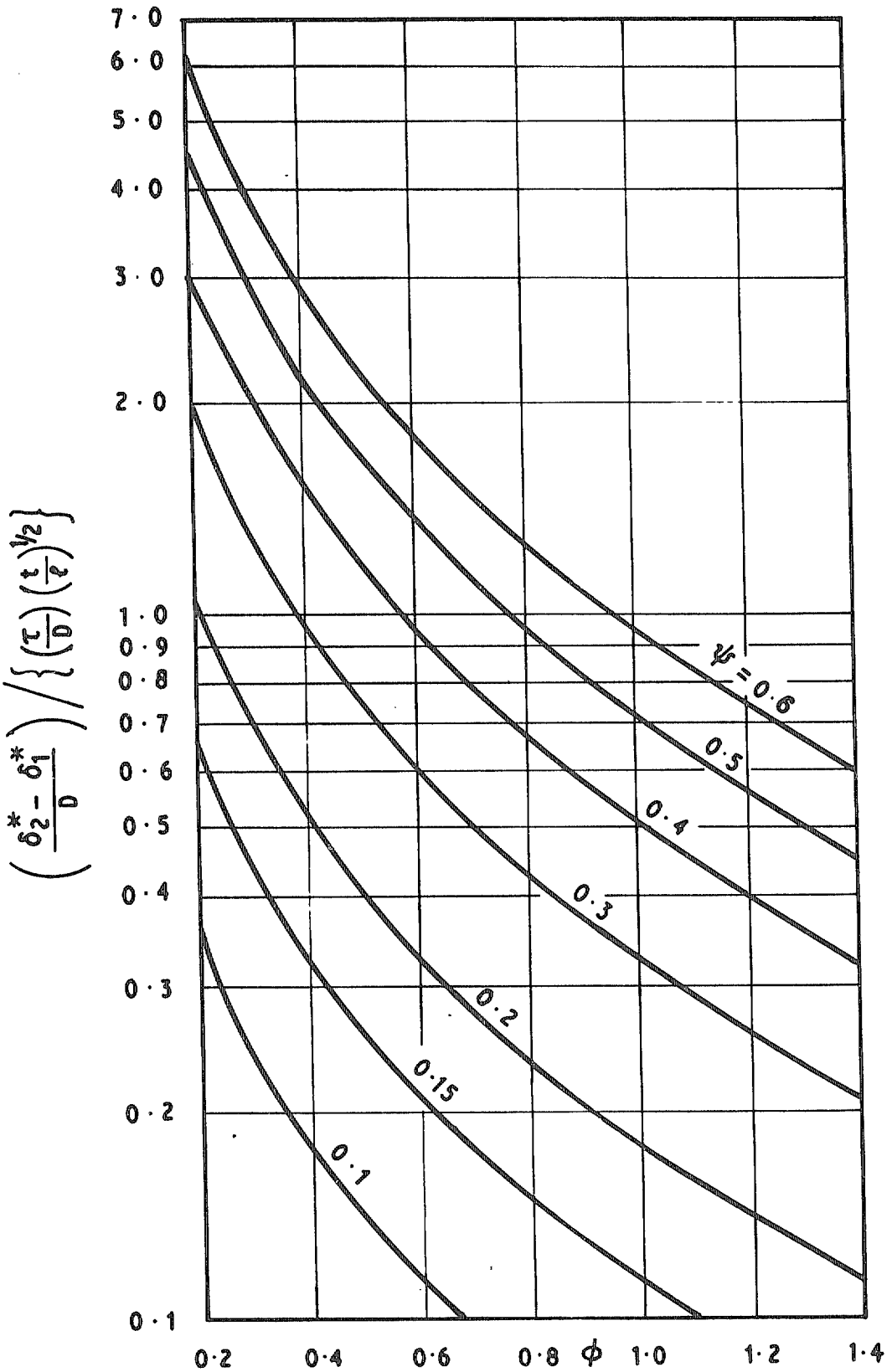

Fig 5 Annulus boundary layer displacement thickness increase due to tip leakage for fans with given duty coefficients (ϕ, ψ)

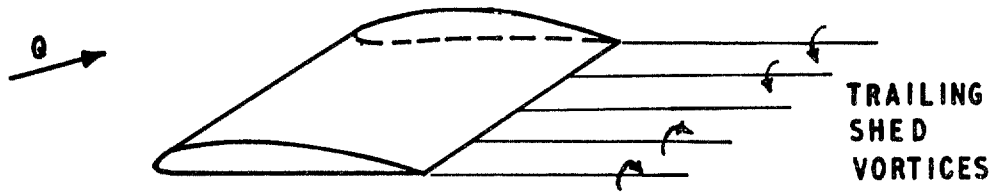

(A) VORTEX LATTICE METHOD

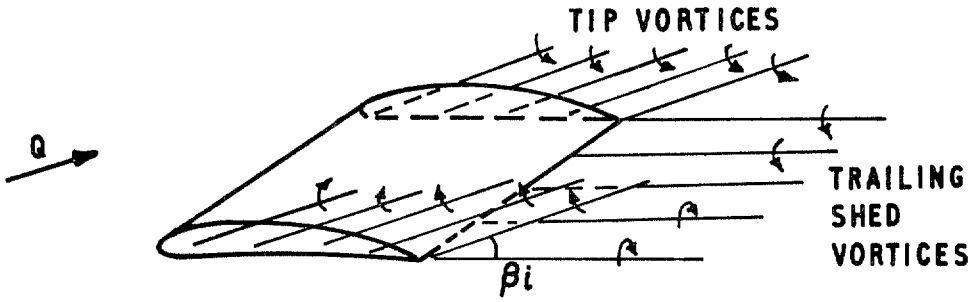

(B) TIP VORTEX METHOD

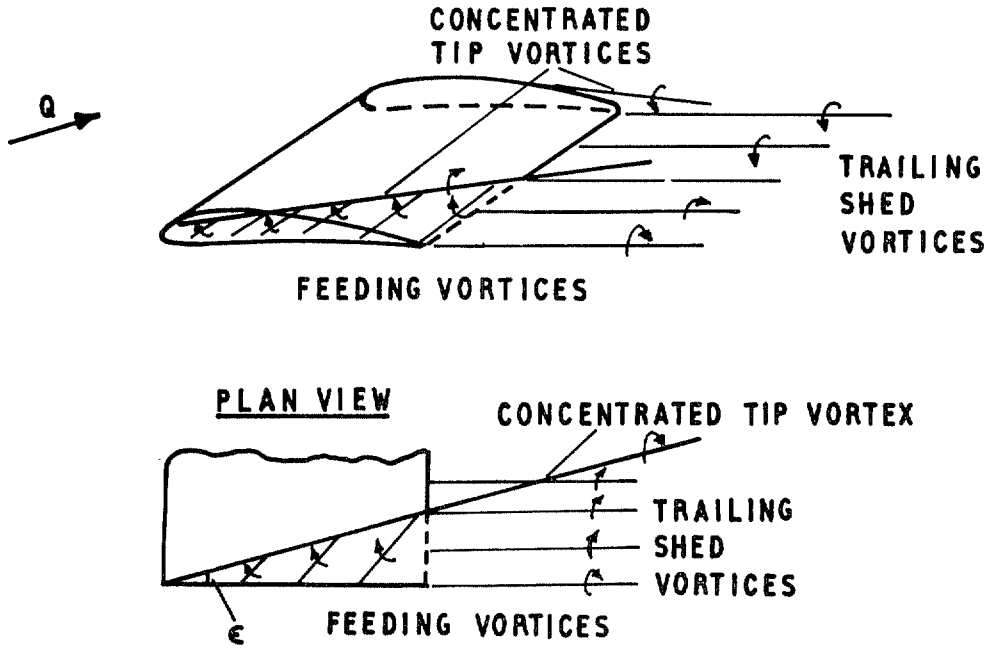

(C) CONCENTRATED TIP VORTEX METHOD

Fig 6a-c Diagrammatic view of different models

Fig 7

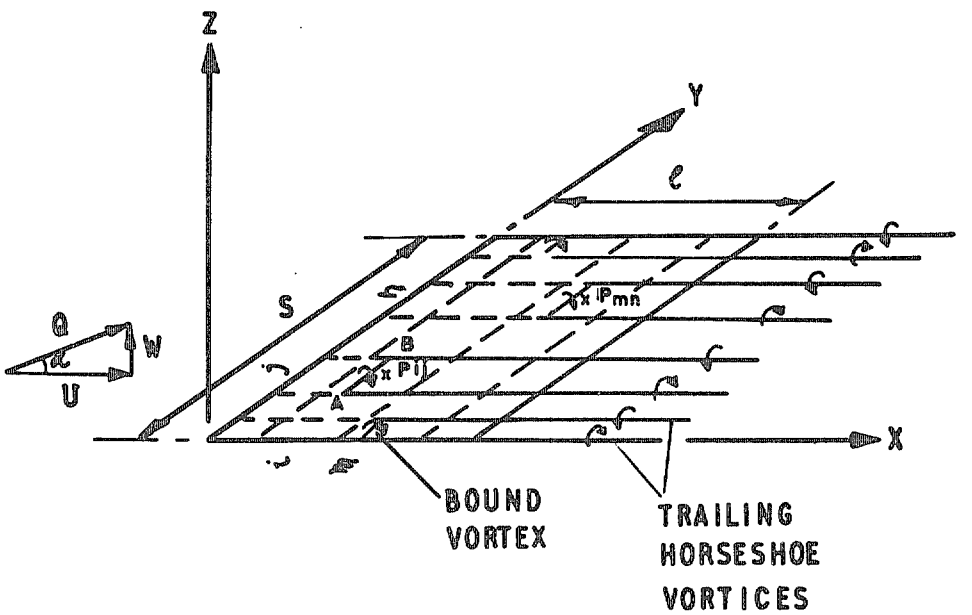

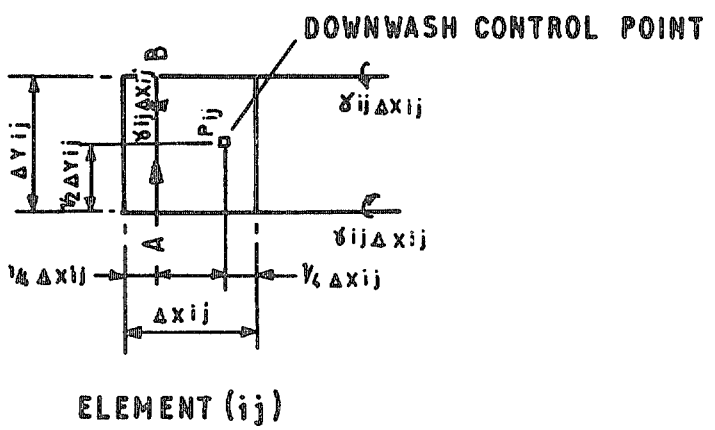

Fig 7 Vortex model for vortex lattice method

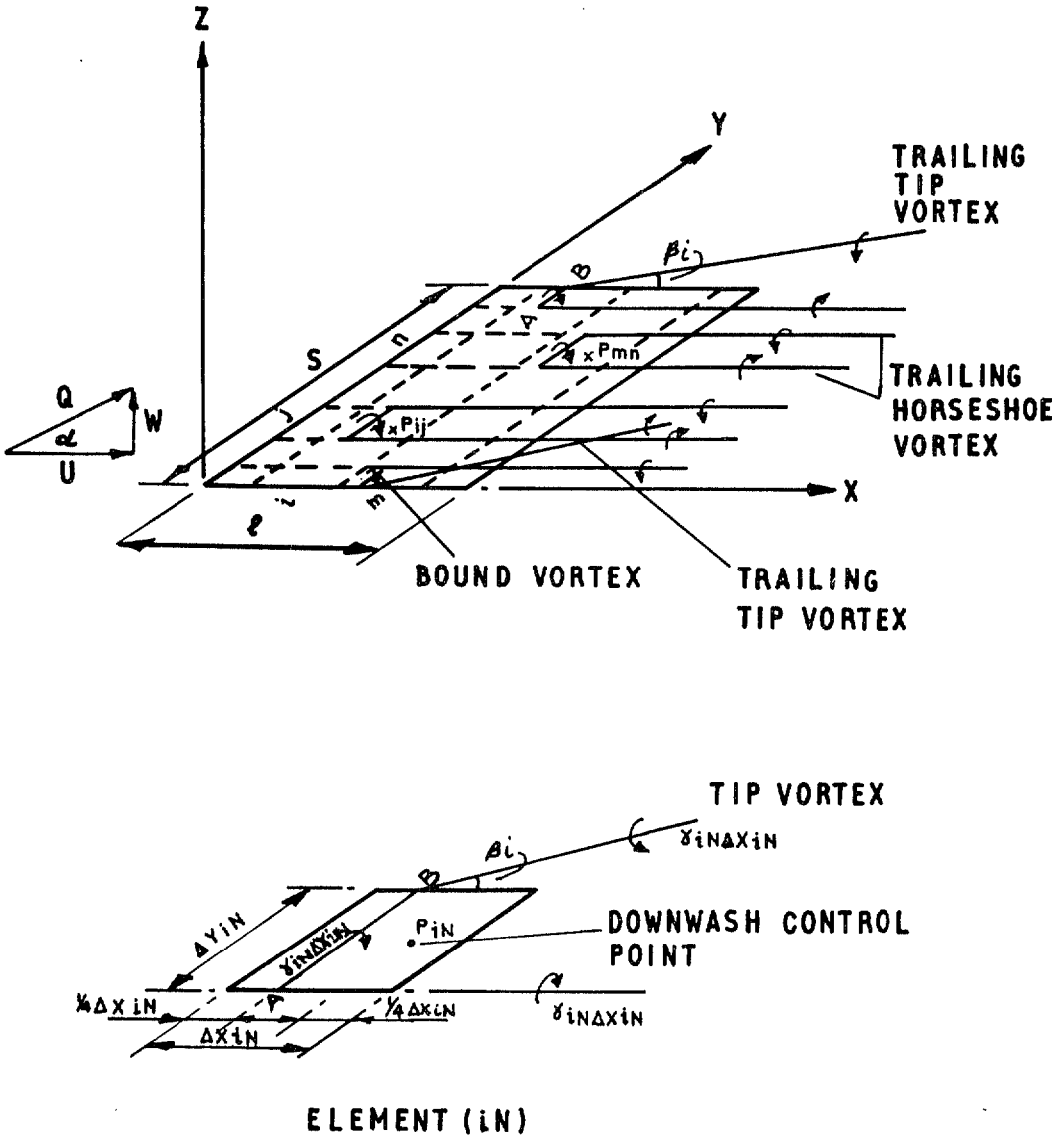

Fig 8 Vortex model for tip vortex method

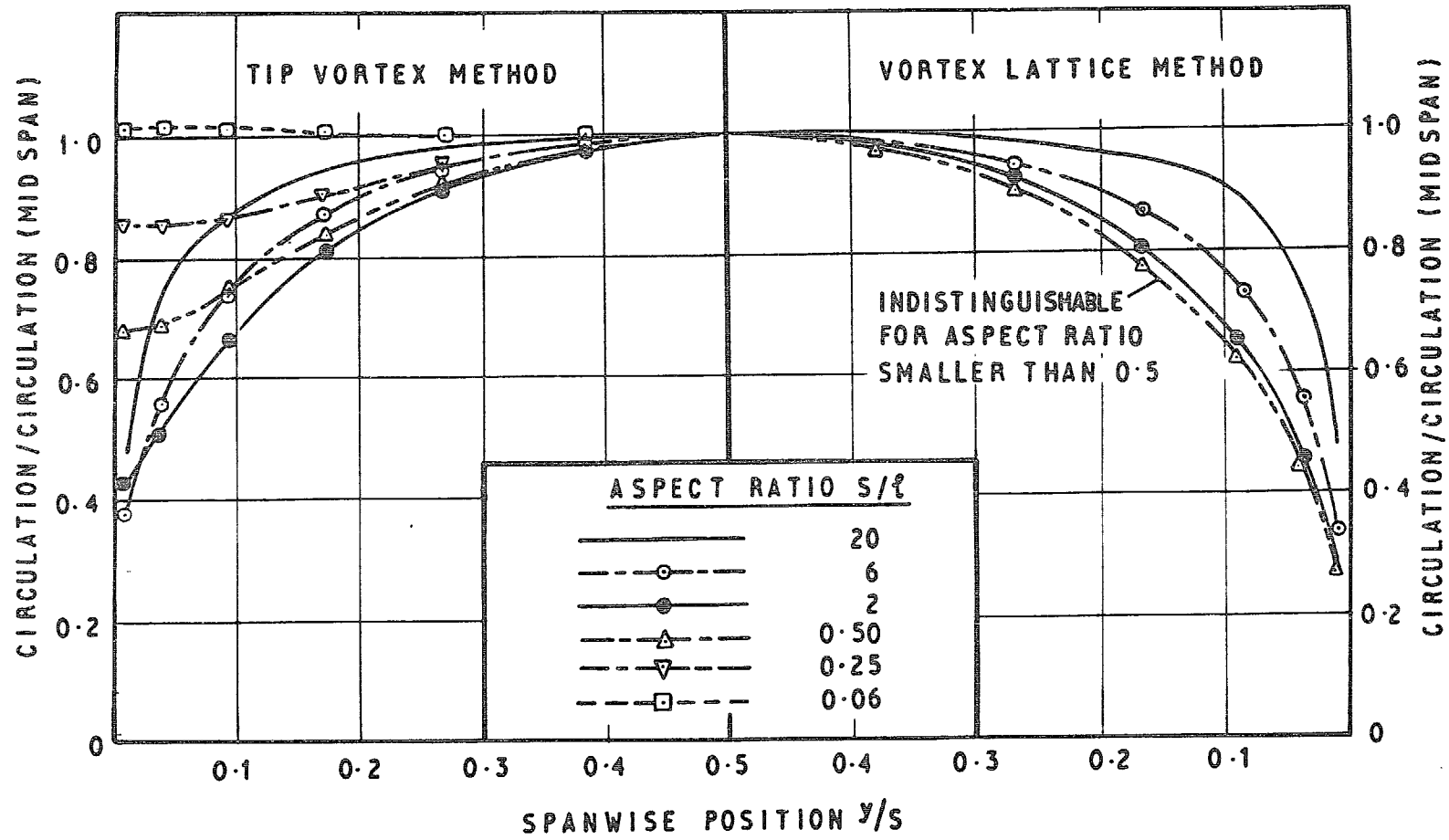

Fig 9 Variation of circulation along span for flat plate aerofoils at 4° incidence

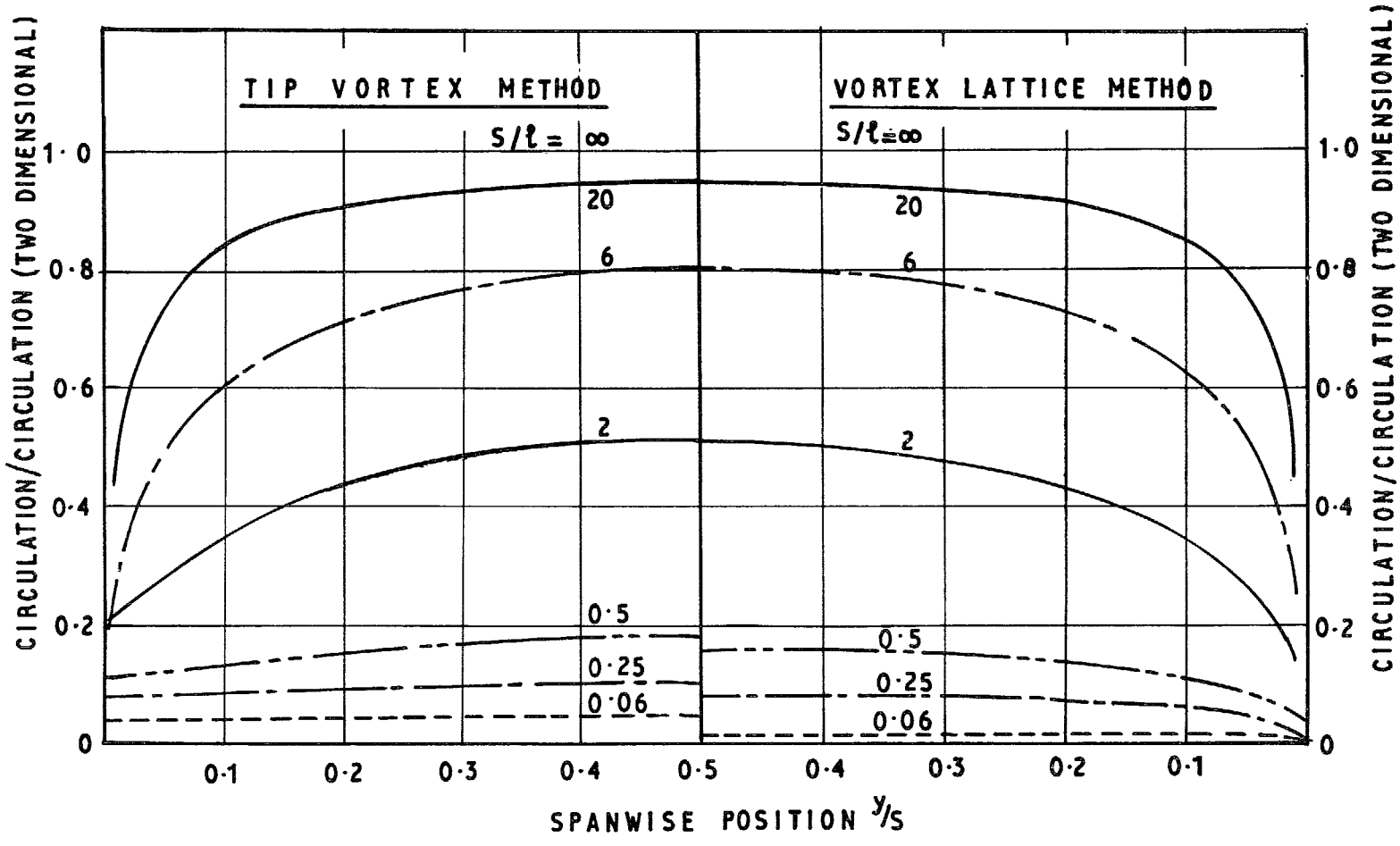

Fig 10 Variation of circulation along span for flat plate aerofoils at 4° incidence

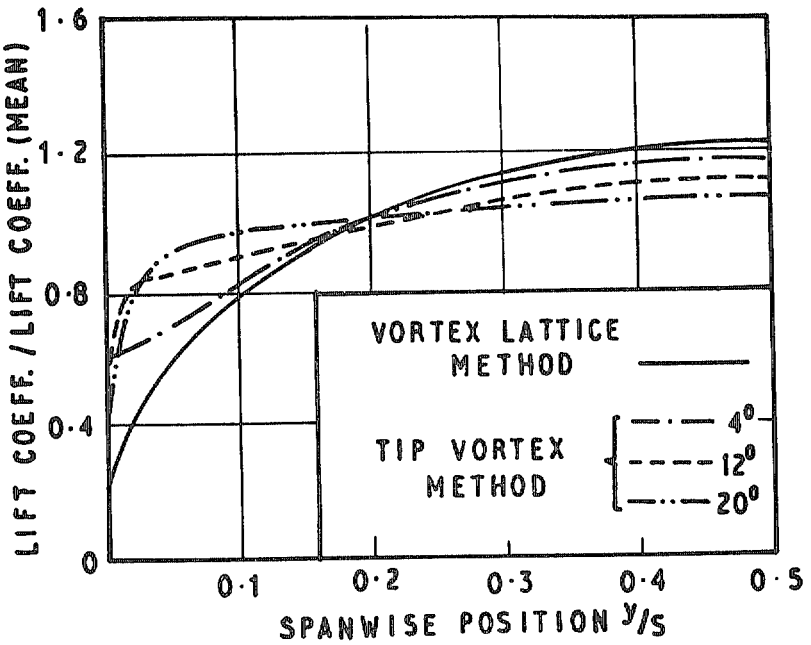

Fig 11 Variation of lift coefficient with incidence $s/\ell = 1.0$

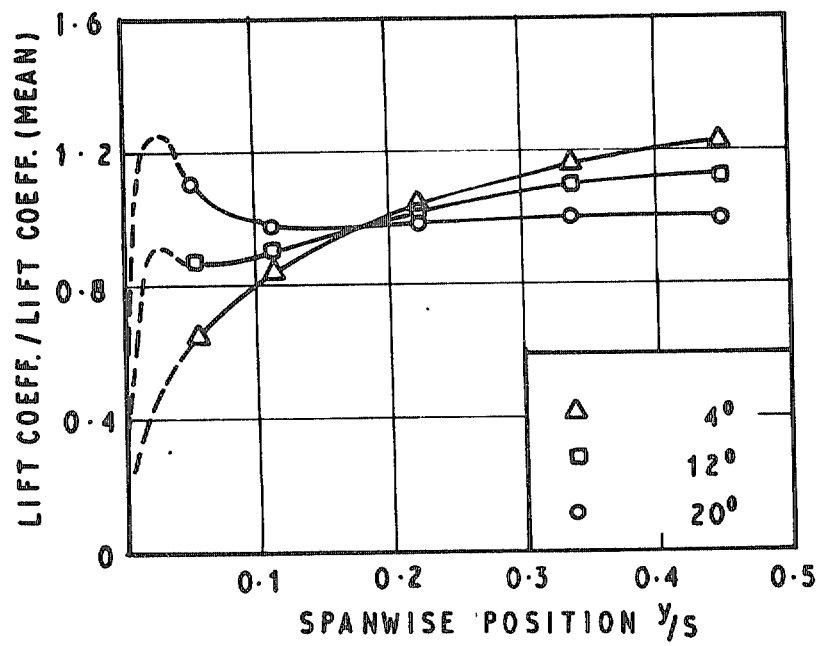

Fig 12 Experimental[7] variation of lift coefficient with incidence $s/\ell = 1.0$

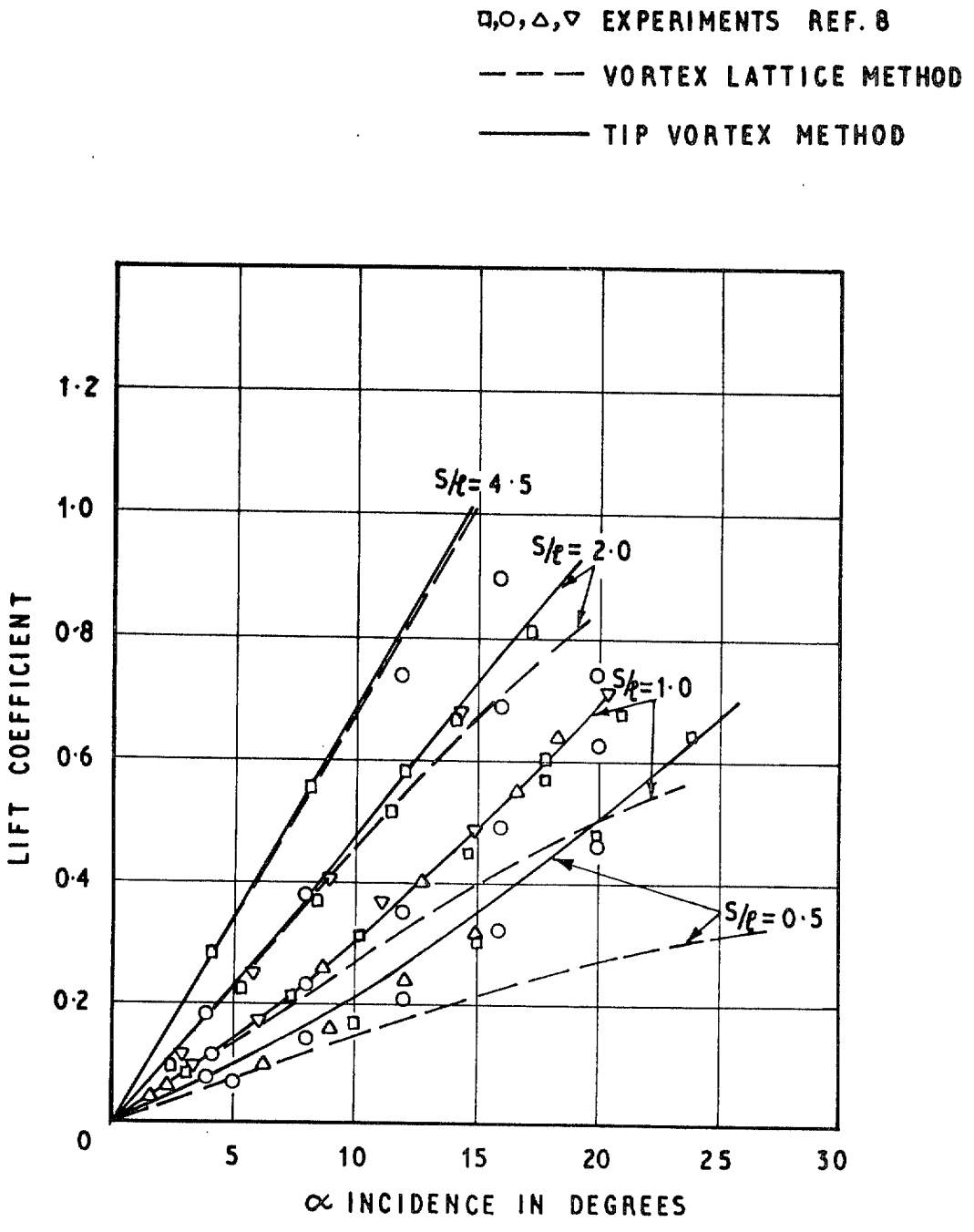

Fig 13 Comparison between experimental and theoretical lift coefficient for flat plate aerofoils

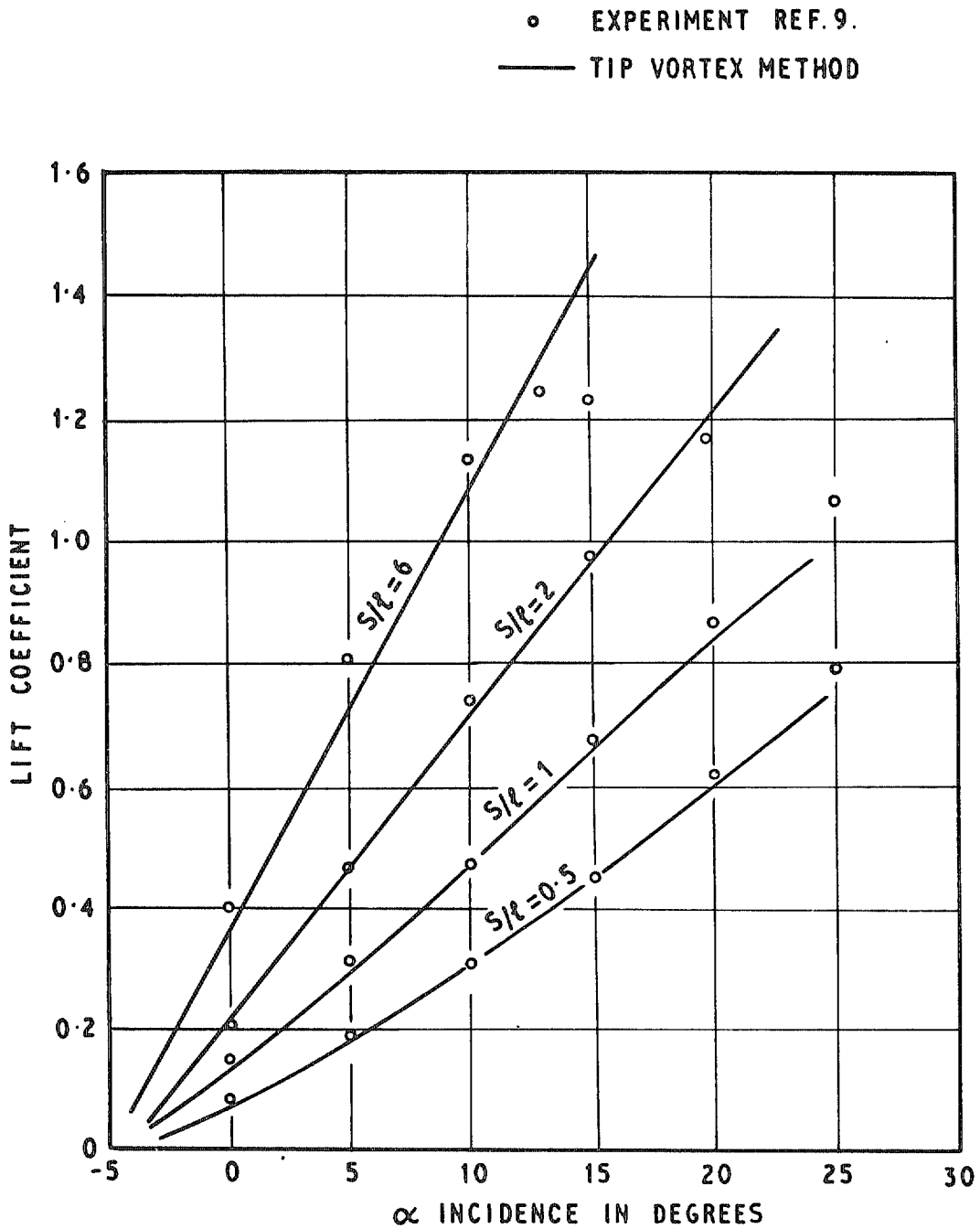

Fig 14 Comparison between experimental and theoretical (TVM) lift coefficient for Clark-Y aerofoils at different angle of incidence

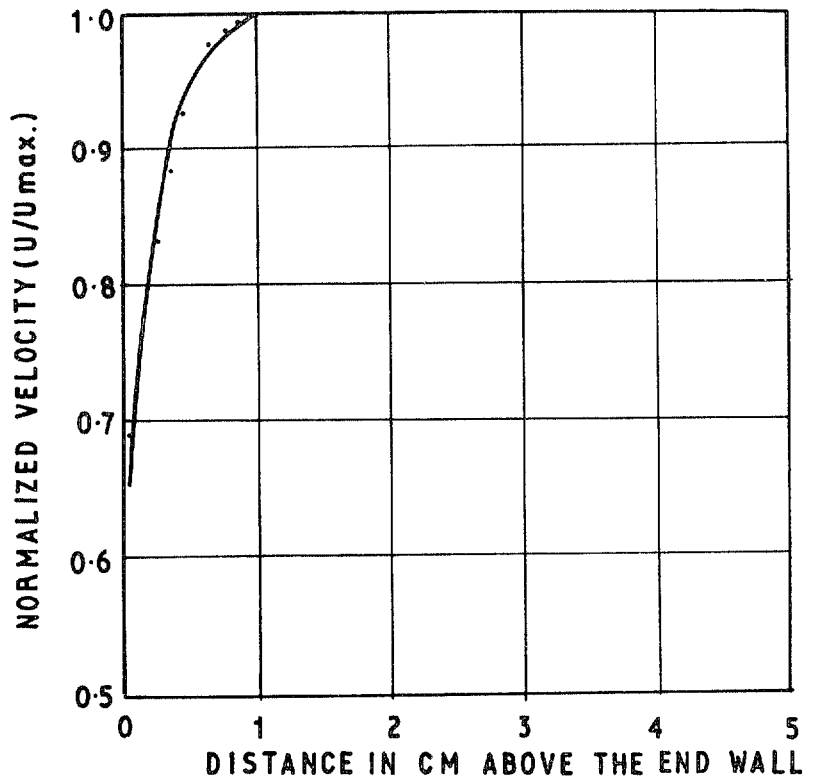

Fig 15a Velocity profile – experiment A

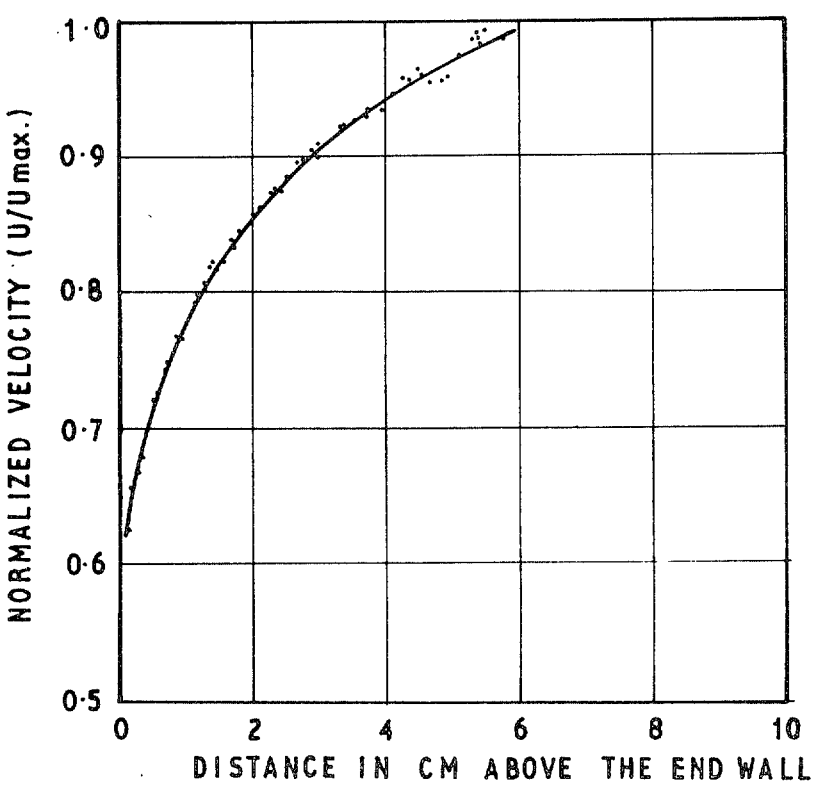

Fig 15b Velocity profile – experiment B

Fig 16

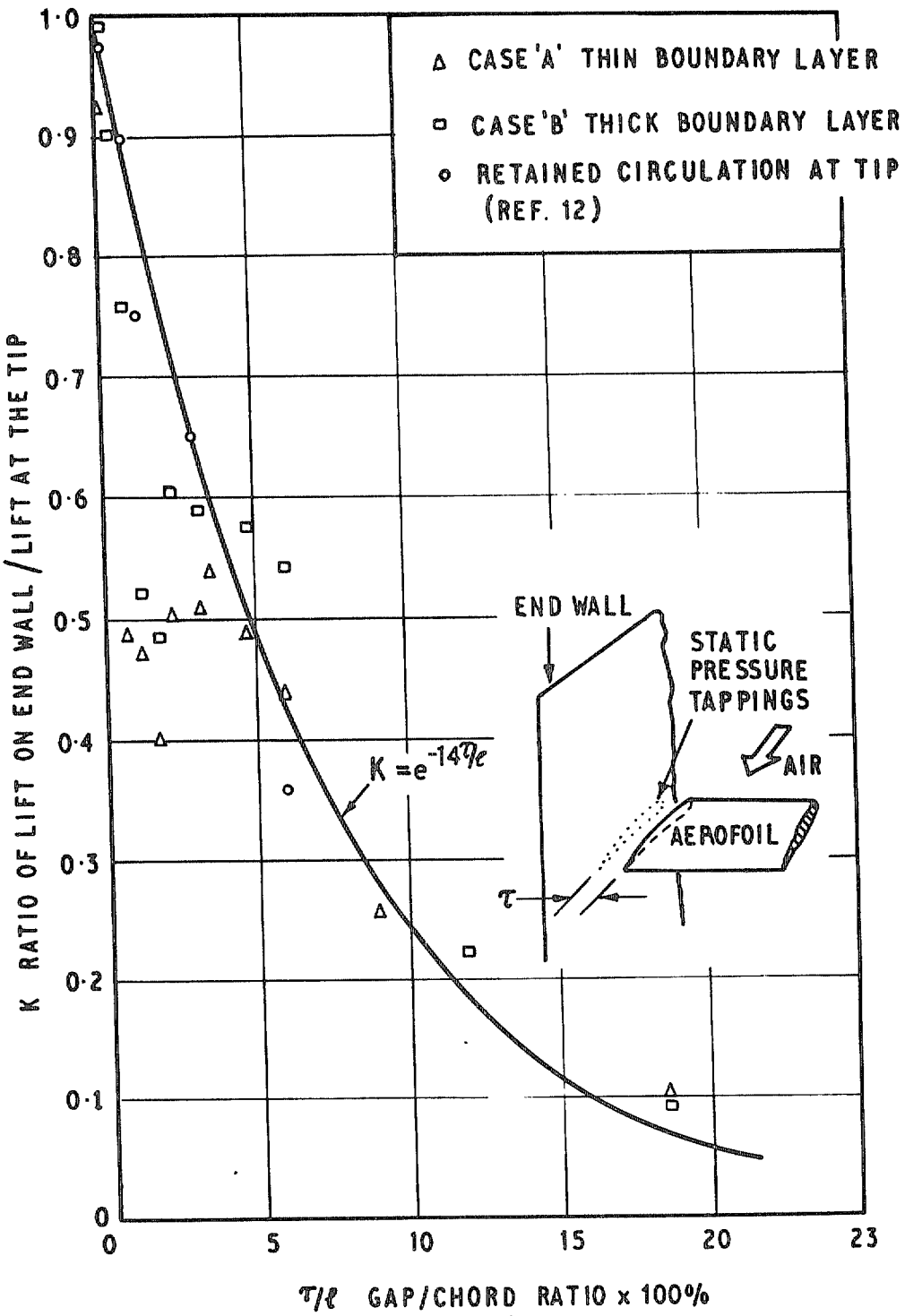

Fig 16 Ratio of lift on the end wall to the lift at the tip with gap/chord ratio

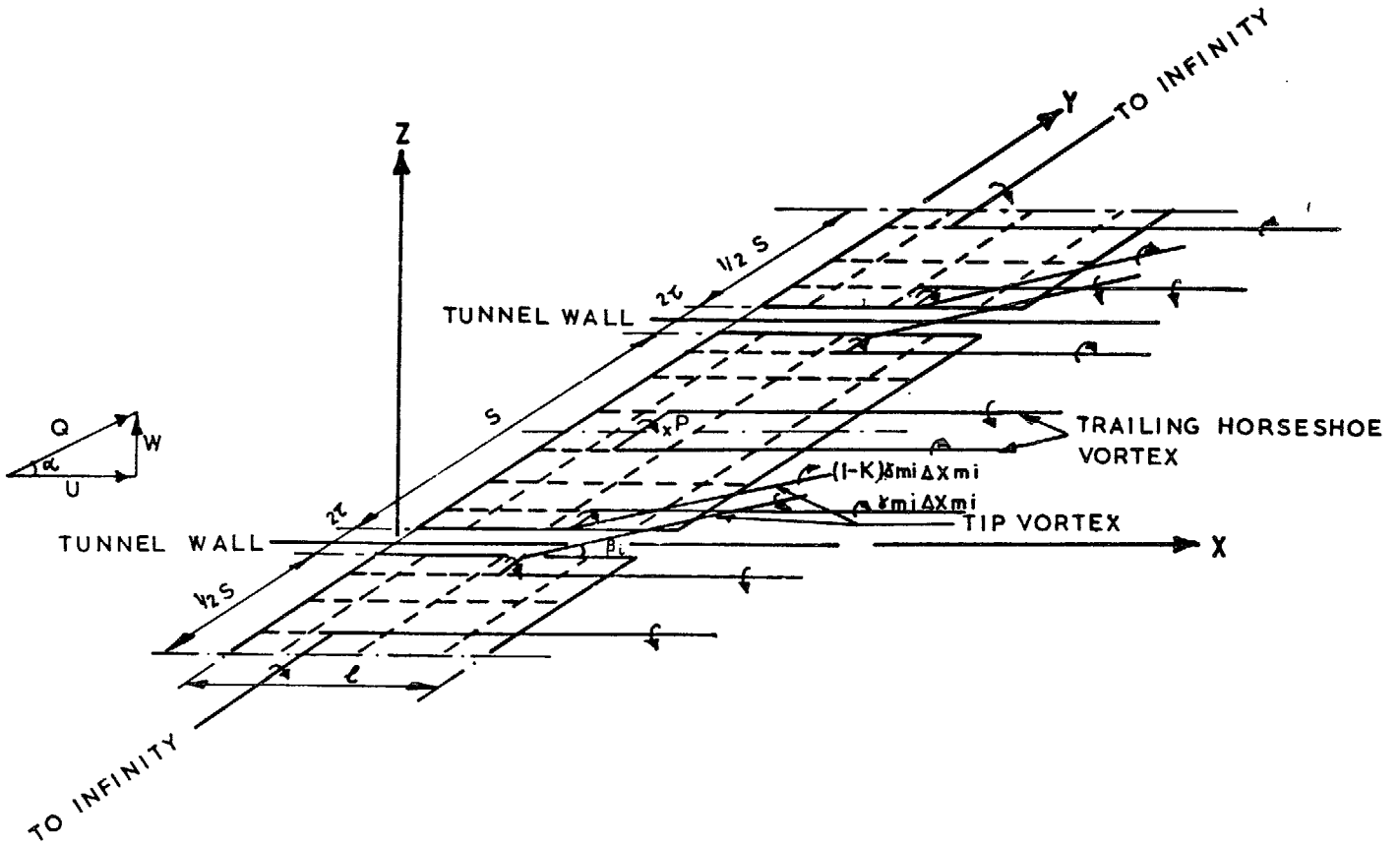

Fig 17 Vortex model for tip clearance calculation modified tip vortex method

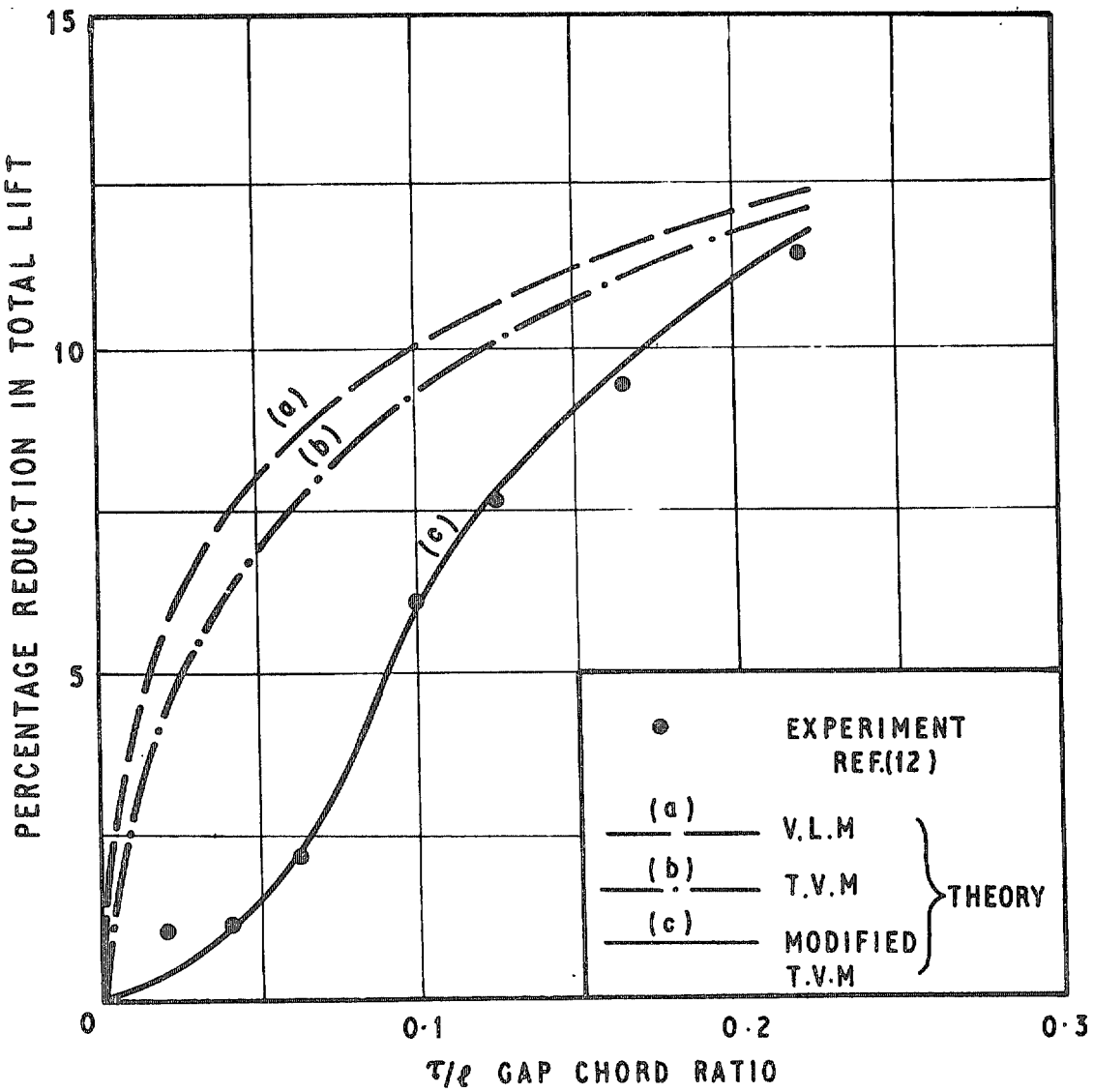

Fig 18 Comparison between experimental and theoretical reduction in total lift for various gap/chord ratios

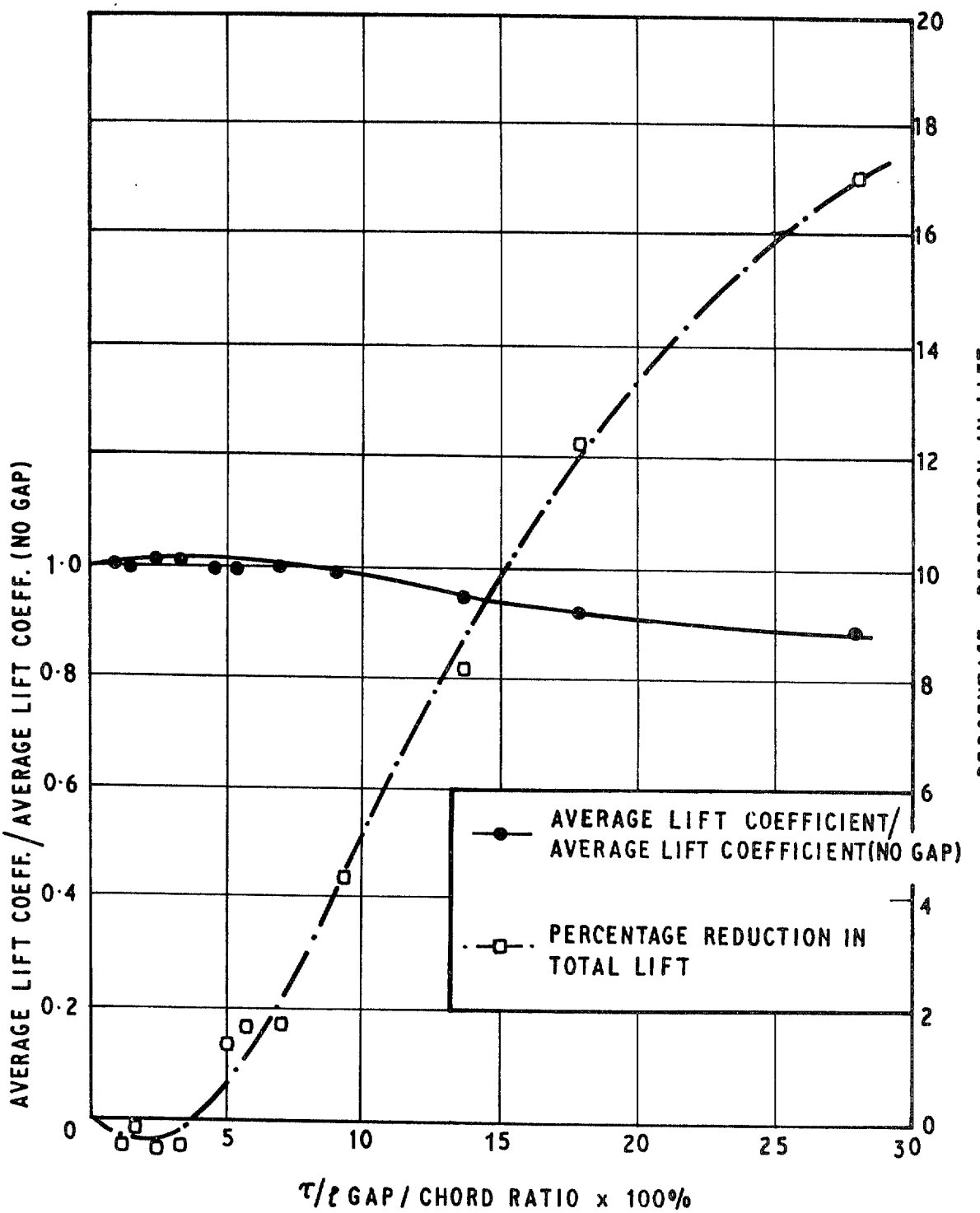

Fig 19 Variation of lift and average lift coefficient with gap/chord ratio (case A)

Fig 20

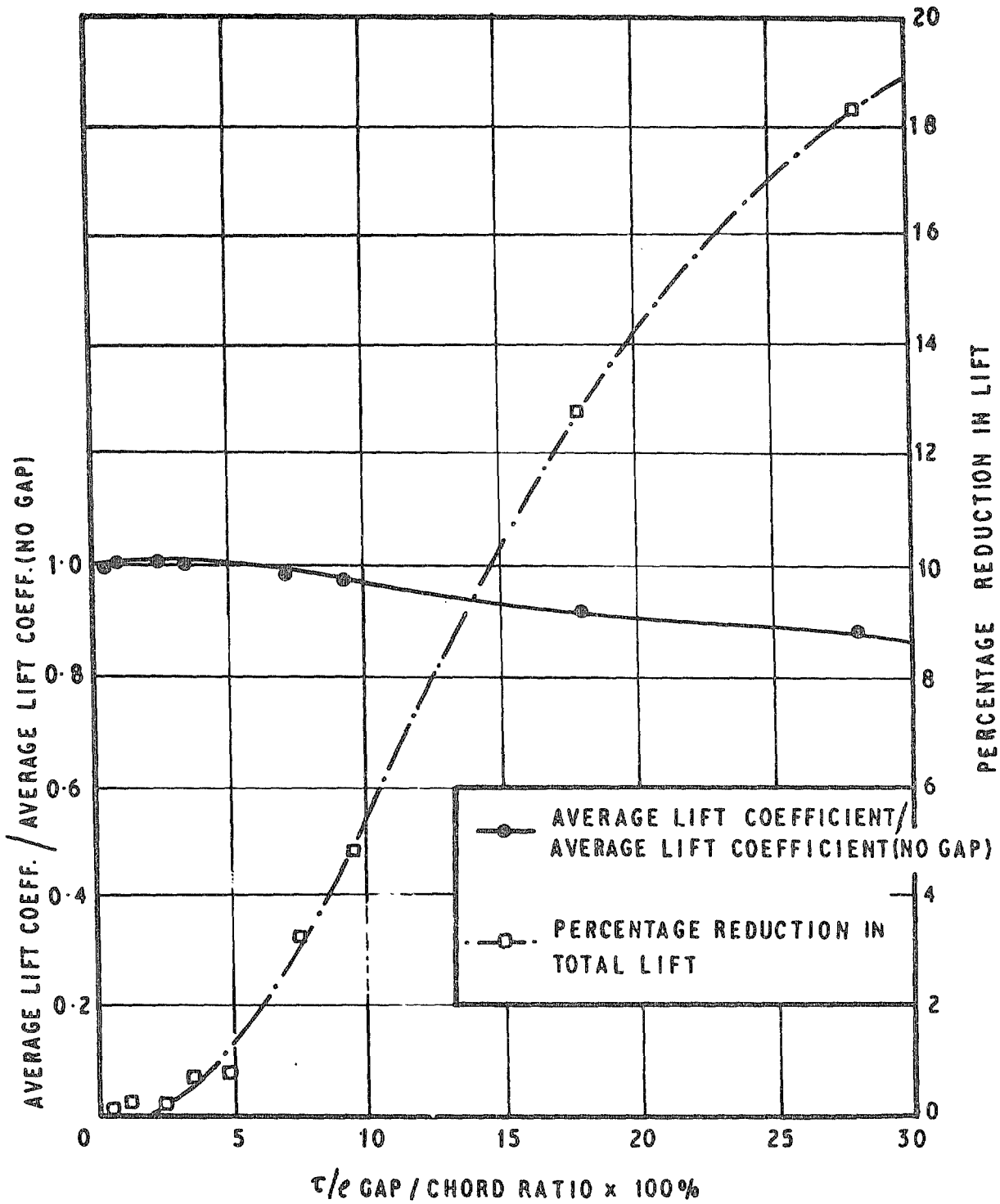

Fig 20 Variation of lift and average lift coefficient with gap/chord ratio (case B)

Printed in England for Her Majesty's Stationery Office by the Royal Aircraft Establishment, Farnborough. Dd. 586386 K4 10/78.

First published 1979

HER MAJESTY'S STATIONERY OFFICE

Government Bookshops
49 High Holborn, London WC1V 6HB
13a Castle Street, Edinburgh EH2 3AR
41 The Hayes, Cardiff CF1 1JW
Brazennose Street, Manchester M60 8AS
Southey House, Wine Street, Bristol BS1 2BQ
258 Broad Street, Birmingham B1 2HE
80 Chichester Street, Belfast BT1 4JY

Government Publications are also available through booksellers

R &M No.3829
ISBN 0 11 471162 3